Hydrogeological control of the thermal regime of a sub-alpine headwater stream

Benjamin Roesky[1] and Masaki Hayashi[2]

[1]BGC Engineering Inc
[2]University of Calgary

May 5, 2021

Abstract

Stream thermal regimes are critical to the stability of freshwater habitats. There is growing concern that climate change will result in stream warming due to rising air temperatures, decreased shading in forested areas due to wildfires, and changes in streamflow. Groundwater plays an important role in controlling stream temperatures in mountain headwaters, where it makes up a considerable portion of discharge. This study investigated the controls on the thermal regime of a headwater stream, and the surrounding groundwater processes, in a catchment on the eastern slopes of the Canadian Rocky Mountains. Groundwater discharge to the headwater spring is partially sourced by a seasonal lake. Spring, stream, and lake temperature, water level, discharge and chemistry data were used to build a conceptual model of the system. Meteorological data was used to set up a stream temperature model. A tracer test was carried out to estimate hyporheic exchange along the study reach. This study presents a unique example of an indirectly lake-headed stream i.e., where the interaction of groundwater and lake water, and the hydraulic gradient determine the resulting stream temperature. Energy balance of the stream is mainly controlled by radiation. Sensible and latent heat fluxes play a secondary role, but their effects generally cancel out. Hyporheic exchange is present but plays only a minor role in the energy balance. During snowfall events, the latent heat associated with melting of direct snowfall onto the water surface was responsible for rapid stream cooling. An increase in advective inputs from groundwater and hillslope pathways did not result in observed cooling of stream water during rainfall events. The results from this study will assist water resource and fisheries managers in adapting to stream temperature changes under a warming climate.

Hydrogeological control of the thermal regime of a sub-alpine headwater stream

Benjamin Roesky and Masaki Hayashi

Department of Geoscience, University of Calgary

To be submitted to *Hydrological Processes* (< 7500 words).

Abstract (< 300 words)

Stream thermal regimes are critical to the stability of freshwater habitats. There is growing concern that climate change will result in stream warming due to rising air temperatures, decreased shading in forested areas due to wildfires, and changes in streamflow. Groundwater plays an important role in controlling stream temperatures in mountain headwaters, where it makes up a considerable portion of discharge. This study investigated the controls on the thermal regime of a headwater stream, and the surrounding groundwater processes, in a catchment on the eastern slopes of the Canadian Rocky Mountains. Groundwater discharge to the headwater spring is partially sourced by a seasonal lake. Spring, stream, and lake temperature, water level, discharge and chemistry data were used to build a conceptual model of the system. Meteorological data was used to set up a stream temperature model. A tracer test was carried out to estimate hyporheic exchange along the study reach. This study presents a unique example of an indirectly lake-headed stream i.e., where the interaction of groundwater and lake water, and the hydraulic gradient determine the resulting stream temperature. Energy balance of the stream is mainly controlled by radiation. Sensible and latent heat fluxes play a secondary role, but their effects generally cancel out. Hyporheic exchange is present but plays only a minor role in the energy balance. During snowfall events, the latent heat associated with melting of direct snowfall onto the water surface was responsible for rapid stream cooling. An increase in advective inputs from groundwater and hillslope pathways did not result in observed cooling of stream water during rainfall events. The results from this study will assist water resource and fisheries managers in adapting to stream temperature changes under a warming climate.

Keywords (eight required)

Stream temperature, alpine hydrology, energy balance, groundwater-stream interaction, headwater spring, seasonal lake, hyporheic exchange, Canadian Rockies

1. Introduction

The temperature of water plays a critical role in the stability of various habitats including those of freshwater fish (Ebersole, Liss, & Frissell, 2001). The major energy fluxes that determine stream temperatures are net shortwave and longwave radiation, sensible and latent heat transfer, bed heat conduction, advection by groundwater, and hyporheic exchange (Moore, Sutherland, Gomi, & Dhakal, 2005). These can be classified as exchanges occurring at either the air/water interface or the streambed/water interface (Caissie, 2006). Energy-balance studies have found that net streambed heat fluxes make up a greater fraction of the total heat budget for smaller streams. In a catchment in New Brunswick, Canada, the streambed heat flux accounted for 23 % of the total heat flux for a smaller stream compared to 12 % for a larger stream (Hebert, Caissie, Satish, & El-Jabi, 2011). In a headwater stream, in British Columbia, hyporheic exchange accounted for up to 25 % that of net radiation during the period of the day with the greatest warming rate (Moore et al., 2005a). However, the streambed heat fluxes vary both spatially and temporally within the channel (Caissie & Luce, 2017). Groundwater discharge results in summer stream cooling and winter stream heating, acting as a buffer from thermal extremes (Hayashi & Rosenberry, 2002). Within the stream channel, patterns of seepage flux are determined by channel profile and morphology, such as pool and riffle sequences and cross-channel gradients (Gariglio, Tonina, & Luce, 2013).

There is growing concern that climate change will result in stream warming due to rising air temperatures, decreased shading in forested areas due to wildfires, and changes in streamflow (Leach & Moore, 2010). Long-term monitoring data have already shown stream temperature increases over the last 30 years across the northwestern United States (Isaak, Wollrab, Horan, & Chandler, 2012). In mountain regions, changes to flow regimes due to changing snowmelt dynamics (Bavay, Grünewald, & Lehning, 2013), and rising groundwater temperatures must also be considered (Kurylyk, MacQuarrie, & McKenzie, 2014). Previous work has revealed that groundwater, as distinguished from recent seasonal precipitation and meltwater inputs, makes up an important fraction of mountain headwater discharge (Hood & Hayashi, 2015). Estimates vary across catchments and seasons; up to 60 % of streamflow, during early snowmelt, was attributed to groundwater in a catchment in the Colorado Rocky Mountains (Liu, Williams, & Caine, 2004). In the Canadian Rockies, a rock glacier spring contributed up to 50 % of streamflow during summer baseflow periods and up to 100 % of streamflow over winter (Harrington, Mozil, Hayashi, & Bentley, 2018). The relative position and size of alpine aquifers, including rock glacier; moraine; talus; and alpine meadow, determine the groundwater storage-discharge characteristics in these catchments (Hayashi, 2020).

There have been few studies on the effects of groundwater discharge on the temporal and spatial variability in alpine thermal regimes. Consequently, the impact of groundwater on ecosystems in these settings is poorly understood (Brown, Milner, & Hannah, 2007). The few existing studies characterize the different source water contributions including snowmelt, glacial icemelt and groundwater (Brown, Hannah, & Milner, 2005). Groundwater-fed alpine streams exhibit greater streamflow permanency (Brown, Hannah, & Milner, 2006) and dampened diurnal temperature variations (Constantz, 1998). Discrete groundwater discharge, such as from a rock glacier spring, can mitigate the warming effect of lake outflows, serving as a thermal refuge under a warming climate (Harrington, Hayashi, & Kurylyk, 2017).

Direct precipitation onto the stream surface is an advective component of stream energy balance (Webb & Zhang, 1997). However, most studies do not include this flux, (e.g., Garner, Malcolm, Sadler, Millar, & Hannah, 2015; Harrington et al., 2017; Moore, Spittlehouse, & Story, 2005) citing a study showing it to be negligible, even during heavy rain (Evans, McGregor, & Petts, 1998). However, there are evidences indicating that stream temperatures do respond to precipitation events. Brown and Hannah (2007) attribute observed temperature responses in an alpine stream to 'advected energy inputs, primarily from surface and near-surface hillslope pathways and by groundwater, rather than direct heat flux by falling precipitation'. The idea that precipitation results in stream cooling due to the corresponding flow generation processes is repeated elsewhere, where direct precipitation accounted for less than 1.2% of the daily total heat flux and could not account for observed cooling (Hebert et al., 2011). However, these studies did not consider the effects of solid precipitation which could have a larger impact on the energy balance. To our knowledge, Leach and Moore (2017) were the first to demonstrate the role of channel-intercepted snowfall on stream temperatures. Little work has been done to date to quantify the processes that lead to observed stream temperature cooling during precipitation events.

The aim of this study is to improve and quantify our understanding of the processes controlling the thermal regimes of groundwater-fed headwater streams in mountain regions. The three main study objectives are:

1. Determine the spatial and temporal variability in groundwater discharge temperature to a sub-alpine stream and develop a conceptual model for the system.
2. Quantify the solid precipitation induced stream cooling processes to improve stream temperature models.
3. Characterize the downstream changes in the first-order stream channel by quantifying transient storage and increases in discharge.

2. Study Site

The study is conducted at an unnamed headwater stream in a valley called Hathataga (meaning huckleberry) by the local Stoney people (Crawler, Labelle, Mark, & Willie, 1987). Therefore, in this study the stream is called Hathataga Creek. It is located in the Fortress Ski Area (50°49'14" N, 115°12'50" W) in Alberta, on the eastern slopes of the Canadian Rocky Mountains. The stream starts at a set of perennial outlet springs (Gauging Station 1 (GS1); Figure 1B) and flows north until it merges with Galatea Creek. The focus of this study is on an 850 m long reach extending from the outlet springs to a previously installed stream gauging station (GS4; Figure 1B).

A tarn, with no surface water outflows, is located at a higher elevation to the south of the springs, separated by a moraine. The tarn, referred to in this study as Hathataga Lake, forms following snowmelt and dries up by late summer (Christensen, Hayashi, & Bentley, 2020). As a result of the hydraulic gradient, the springs drain the sub-catchment that includes the tarn. This means that in summer months water flows from Hathataga Lake to the springs.

The spring system consists of numerous discrete discharge points that combine to form three spring branches (S1, S2 and S3) that merge just above GS1. The location and presence of these transient discharge points is dependent on the elevation of the water table. It is important to distinguish between lake-headed streams and headwater streams as downstream temperature gradients reflect source water temperature (Mellina, Moore, Hinch, Macdonald, & Pearson, 2002). Hathataga Creek is indirectly lake-headed because there is no surface water connection to Hathataga Lake. Another study at the site determined a travel time from the lake to the spring system of approximately 4 hours, using a tracer test (He, J., 2021). Given the horizontal distance of approximately 100 m the hydraulic conductivity of the moraine is on the order of 1×10^{-2} m s^{-1}.

Elevations in the catchment range from 2034 m.a.s.l at the lower gauging station (GS4) to 2900 m.a.s.l at the southern headwall. The catchment has been divided into four sub-catchments (W1 to W4) (Figure 1A).

The bedrock underlying Hathataga Lake and the study reach consists of recessive shales of the Jurassic

Fernie Formation (McMechan, 2012). The ridges between these valleys are made up of Paleozoic carbonates. The Sulphur Mountain Thrust separates the Fernie Formation from the older, more resistant carbonates that make up the headwall in the southern and western part of the study catchment (Figure 1A).

Surficial sediments and the geomorphology of the area can be attributed to the late Pleistocene and Holocene glaciations (Beierle, Smith, & Hills, 2003), which have resulted in the north facing cirque that can be seen today, along with extensive moraine deposits surrounding Hathataga Lake. Freeze-thaw weathering of the carbonate headwall has and continues to contribute to steep talus cones. The coniferous tree line extends to the base of these talus cones.

The outlet springs discharge at the base of the moraine north of the lake. Stream geomorphology changes considerably downstream (Figure 2) (Roesky, 2020). Flow is often turbulent passing through countless pools and riffles. Between the outlet springs and GS2, the western stream banks are shallow with numerous visible bank seeps. The eastern stream banks are typically steeper, incised by 1 to 2 m, with bedrock only occasionally outcropping. The hillslopes are mostly tree covered but some segments are covered in alpine meadow on the western side. Downstream of GS2 the stream gets progressively more incised, by up to 10 m, with increasing bedrock exposure on both sides (Figure 2). Stream meanders also become more frequent.

3. Methods

3.1 Stream discharge and temperature

Stream discharge was manually measured bi-weekly (May-August) or monthly (September-April) using a horizontal-axis current meter (Global Water, FP101) and the velocity-area method (Dingman 2002, p. 609) with an expected uncertainty of up to 9 % (Hood, Roy, & Hayashi, 2006). A stage-discharge rating curve was developed at each of the four stream gauging stations (GS1 to GS4; Figure 1) using at least ten measurements. A root mean squared error below 0.015 m^3s^{-1} was obtained at all four gauging stations with the largest errors occurring during the baseflow period. Water levels were measured by pressure transducers (Solinst, Levelogger). A continuous discharge record was computed by applying the rating curves to the transducer data.

A number of different instruments were used to measure water temperatures to reflect the spatial and temporal scales of interest. Manual measurements were taken with a hand-held thermocouple thermometer (Omega engineering, HH-25TC) during three spring temperature surveys and for verifying continuous data. Temperature sensors (Maxime Integrated, Ibuttons DS1921Z), coated in rubber (Plasti Dip) for waterproofing, were used to measure longitudinal stream temperature profiles (T1 to T11), spring branch temperatures (S1 to S3), and the temperature of the Western tributary (T12). The thin rubber coating allowed the sensors to reach thermal equilibrium in under 5-minutes. Each temperature sensor was tied to a nail that was hammered into the streambed. A flat rock was rested on each nail head to shield the sensor from solar radiation. The pressure transducers (Solinst, Levelogger) also recorded temperatures in the lake and at the stream gauging stations. Manufacturer-specified accuracies are ±1°C and ±0.05°C for the *Ibuttons* and*Leveloggers* respectively. The accuracy of the *Ibuttons* was improved to ±0.25°C following the method outlined in Johnson et al. (2005). Sensors were calibrated in a constant temperature bath (VWR, 1157 Polyscience Refrigerated Circulator) over the range of temperatures observed in the field. Streambed temperature was also monitored by an*Ibutton* , installed in P1 (Piezometer 1), 40 cm below the streambed (Figure 1).

Snapshots of stream surface temperature were captured with a thermal infrared camera (FLIR, E95). The manufacturer-listed accuracy is ± 2 °C and the thermal sensitivity is 0.04 °C. A programmable emissivity of 0.96 was used along with measured relative humidity and air temperature.

3.2 Meteorological conditions

The University of Saskatchewan had previously installed six automatic weather stations (AWS) in the study catchment. In this work, AWS1 located in the meadow by the outlet springs was used (2084 m.a.s.l.). It measured cumulative precipitation (Geonor, T-200B, with Alter wind shield), air temperature and relative humidity (Rotronic, HC2-S3), shortwave and longwave radiation (Kipp & Zonen, CNR4) and wind speed (R. M. Young, 05103).

Precipitation phase was determined using an air temperature threshold of 0 °C (Marks, Winstral. Reba, Pomeroy, & Kumar, 2013). Below 0 °C precipitation was classified as snow and above 0 °C as rain. However, since the threshold is site specific (Marks et al., 2013) a time-lapse camera (Wingscapes, TimelapseCam) was used to confirm the classification. The camera was set up by the outlet springs to take photos at 5-minute intervals. The images were then visually inspected to see if snowfall was occurring or if it had accumulated on the ground. This crude method assumes that snowfall does not melt within the 5-minute window, prior to image capture. Furthermore, when snowfall occurred at night, we assume that melt did not occur until after sunrise, due to low air temperatures. This method was suitable for our purpose of qualitatively distinguishing between liquid and solid precipitation.

3.3 Water and snow chemistry

Water samples were collected weekly or bi-weekly at GS1, GS2, GS3 and GS4, and at Hathataga Lake's north shore. Additional sampling included the three spring branches (S1, S2 and S3) (see results below) on August 14 and September 26, 2019. All samples were filtered (0.45 µm) and stored in 20-ml high-density polyethylene scintillation vials. A 'ball-in-funnel type collector' was used to collect liquid precipitation (Prechsl, Gilgen, Kahmen, & Buchmann, 2014). A table tennis ball was placed in a funnel to help seal the sample bottle from evaporation and debris. During rainfall, the ball could float which allowed collection. Snow pits were dug to the ground surface, up to 1.5 m, and sampled at 20 cm intervals on March 27, April 23, May 8, 22, 29 and June 11, 2019. All samples from a single pit were combined into a depth-integrated snowpack sample, which was melted at room temperature and bottled. All samples were refrigerated until analysis.

Samples were analyzed for stable isotope ratios, alkalinity and major ion concentrations. Isotopes were analyzed using cavity-ringdown spectroscopy (Los Gatos Research, Water Isotope Analyzer). The ratios of$^{18}O/^{16}O$ and$^{2}H/^{1}H$ were computed with reference to the Vienna Standard Mean Ocean Water isotopic standard (Coplen, 1995). Precision and accuracy as 1 standard deviation of lab standards are 0.2 ^{2}H. Alkalinity was determined using a spectrophotometer (Gallery, Discrete Analyzer). An ion chromatograph (Metrohm, 930 Compact IC Flex) was used for major ion analysis.

Electrical conductivity (EC) was measured manually using a handheld meter (VWR International, Conductivity/Temperature Meter) for point measurements and for verifying continuous data.

3.4 Tracer test

A single uranine tracer experiment was performed on June 26, 2019 to quantify transient storage between GS1 and GS2. Tracer concentration was chosen based on a previous study by Lautz and Siegel (2007) with similar flow conditions. A peristaltic pump (Solinst, 410) was set up at the top of the reach to release 0.3 g L^{-1} of the fluorescent dye, at 1.4 L min^{-1}, for a total of 27 minutes. Fluorometers (Turner Designs, Cyclops-7F) were deployed at locations F1 and F2 (Figure 1), with shade caps, at the end of the reach and in the stream near P4 (Figure 1). To obtain an accurate relationship between sensor output voltage and dye concentration the fluorometers had previously been calibrated in the laboratory with five concentration standards: 0, 0.5, 4, 100 and 400 ppb of uranine. For the experiment, the fluorometers were connected to dataloggers (Campbell Scientific, CR1000) and set to take measurements at 5 second intervals. The resulting breakthrough curves were then used to calculate total tracer recovered to confirm complete mixing.

The one-dimensional transport model OTIS-P (Runkel, 1998) was used to estimate the transient storage parameters, dispersion coefficient, and stream cross sectional area (see electronic supplement for details) assuming that the flow is at steady state and that uranine is a conservative tracer (Smart & Laidlaw, 1977). The steady-state assumption was justified as there was a change in discharge of less than 6 % at GS1 during the experiment.

3.5 Additional data

Drive-point piezometers (1.9 cm inside diameter) were installed within the second spring branch (P2), below AWS1 (P3), to the west of the stream between GS1 and GS2 (P4) and in the lakebed (P5) (Figure 1). Pressure transducers (In-Situ, MiniTroll, accuracy ˜1 mm) were placed in the piezometers to measure groundwater levels and temperatures. Continuous water level data were verified bi-weekly with manual water-level measurements. Lake water level was measured by a pressure transducer (Solinst, Levelogger, accuracy ±0.3 cm), in a lake stilling well. Stream dimension surveys were completed on June 26 and August 2, 2019 whereby stream depth was recorded every 10 cm along the width of the stream, at 24 separate transects. Twelve transects were located between GS1 and GS2 at approximately 20 m intervals and the remaining 12 transects were located at approximately 50 m intervals between GS2 and GS4. The width of the transects ranged from 1.3 to 4.4 m.

3.6 Stream temperature modeling

Stream temperature data were analyzed using the one-dimensional heat transfer model HFLUX (Glose, Lautz, & Baker, 2017). The following describes a model modification introduced in this study, while a brief summary of HFLUX is presented in an electronic supplement.

In previous studies the direct precipitation flux has been calculated using: $q_p = 1.16\ y_p(T_p - T_w)$ (1) where q_p is the precipitation flux (W m^{-2}), y_p is precipitation (mm h^{-1}), T_p is precipitation temperature (°C), T_w is stream temperature (°C), and 1.16 is a unit conversion factor including the specific heat of liquid water (4.2×10^3 J kg^{-1}°C^{-1}) (Hebert et al., 2011; Marcotte & Duong, 1973). Precipitation temperature is assumed to be equal to air temperature (Marcotte & Duong, 1973).

At high elevation sites and in winter, precipitation often falls in the solid state and melts in streams. To account for the latent heat of fusion in the energy balance calculation, Equation (1) is modified in this study as: $q_p = 1.16\ y_p(T_p - T_w) + 92.8 y_p$ (2)

where the second term represents the effect of the latent heat of fusion (= 3.34×10^5 J kg^{-1} at 0 °C) and unit conversion.

The HFLUX model was calibrated for 12:00 August 14 to 12:00 August 20, 2019, which included a snowfall event. The model was then validated for 12:00 August 20 to 12:00 August 26, 2019. Shading (SF), groundwater temperature ($T_{L\text{-}gw}$) and view to sky coefficient (VTS) were estimated during the calibration process, whilst considering field observations and aerial photographs, as the parameters were not measured directly. Parameter estimation was carried out using a nonlinear, multivariable optimization solver known as fminunc (MathWorks, 2020a) which was integrated with the original code. The objective function was set to minimize the root-mean-squared-error (RMSE) between the measured and modeled stream temperatures.

4. Results

4.1 Stream discharge

At the onset of snowmelt, in late May 2019, discharge increased rapidly by an order of magnitude (Figure 3C). Streamflows were high from June 4 to July 8, after which levels receded. There were several peaks in discharge corresponding to air temperature fluctuations (Figure 3B). Discharge from GS2 and GS3 were combined to represent the combined outflow from W2 and W3. Maxima of 0.24, 0.63 and 0.55 m^3 s^{-1} were attained at GS1, GS2 + GS3 and GS4, respectively. Discharge typically increased by 10 % to 30 % between GS1 and GS2, however during snowmelt this went up to 80 %. Diurnal discharge fluctuations, that became more pronounced downstream, were likely caused by evapotranspiration because daily discharge minima occurred between 14:00 and 15:00 and maxima occurred before sunrise.

Three spring temperature and location surveys were carried out during the 2019 field season (Figure 4). On June 26, 25 discrete springs were identified. By August 7, the number of springs was reduced to 16 and by September 26 to seven. Not only did the number of springs decrease over the season but the springs also moved northward to lower elevations, corresponding with a decline in the water table. The highest elevation spring was at 2086.3 m.a.s.l. on June 16 and at 2083.7 m.a.s.l. on September 26.

Spring temperatures on June 26 ranged from 1.1 to 3.6 °C. On August 7, temperatures increased to 2.1–7°C and on September 26 they decreased to 1.9–3.4°C (Figure 4). The warmest springs were initially concentrated in the south-eastern part of the spring system but moved to the eastern stream bank over the course of the season. On September 26, the warmest spring was also the furthest north. Each of the three snapshots in Figure 4 corresponds to different phases in Hathataga Lake's hydroperiod. In (A) the lake water level (WL) was near its peak (2090.0 m.a.s.l., WL = 1.5 m), in (B) the lake temperature was near its peak (2088.8 m.a.s.l., WL = 0.35 m), and in (C) the lake had dried up (2087.8 m.a.s.l., WL = -0.68 m). Note that WL is the water level with reference to the lakebed.

4.2 Spring temperature

The clusters of springs are grouped into three spring branches (S1, S2, and S3 in Figure 4). Thermal infrared images of the spring area were taken on August 14, 2019 at 12:15 to better visualise mixing of the three spring branches (Figure 5). Water surface temperatures were between 1.1 and 6.2°C. Distinguishable features include a cold side spring (Figure 5A) and a sharp thermal boundary between water originating from S1 and S2/S3. It can also be seen that GS1 is situated on the warmer stream side which must be considered during interpretation of the temperature data from the gauging station.

To better resolve the temporal variability, temperature sensors were placed in each of the three spring branches from June 11 to October 17, 2019 (Figure 6). Data gaps were the result of sensors being exposed to air (August) or full datalogger memory (July). Initial temperatures in the spring branches were equal at ~1.3°C but these rapidly diverged at the onset of snowmelt (Figure 6). The maximum recorded temperature in each spring branch was not reached simultaneously: S2 reached its maximum on July 15 with temperatures remaining high until late August. Temperatures at S1, on the other hand, were rising during this time and reached a maximum on August 22. By mid-September temperatures in S2 were back down to S3 levels. S1 temperatures had still not been reduced to S3 levels by October 17. Diurnal variations are likely due to heating of spring water following surface discharge. This is especially noticeable in S3 as it is the longest spring branch above the temperature sensor.

The observed spatial and temporal variability in spring temperatures was described above. Below, changes in spring temperature and discharge and changes in lake temperature and water level are explored (Figure 7). Note that stream temperature measured at GS1 was used, which was heavily influenced by high temperature discharge (Figure 5A). Even though this does not represent the spring system as a whole it captures the relationship between the lake and springs satisfying the purpose of this study. Additionally, water levels measured in P5 were used to include days when water levels were below the lake stilling well. True lake water levels were up to 5 cm higher than heads measured in the lake piezometer due to the downward flux into the lakebed. The downward head gradient beneath the lake accounts for the differences in readings between the lake piezometer and stilling well. To capture both spring snowmelt and the lake drying up, across two different seasons, the study period extends from May 1 to October 1, 2018 and 2019.

During the 2018 season the water table under the lake rose to the surface on May 18, after the onset of snowmelt. The maximum water level was 1.8 m on June 24, coinciding with a maximum spring discharge of 0.31 m^3 s^{-1} (Figure 7B). After this, spring and lake temperatures increased rapidly until air temperatures dropped on July 18 (Figure 7C). By August 15, the lake had dried up and spring temperatures began to fall (Figure 7B and 7C). There are some key distinctions between the 2018 and 2019 seasons. Snowmelt started two weeks later in 2019 meaning that water levels reached the surface on May 31. Snowpack, measured at AWS1, prior to snowmelt was 60 cm deeper in 2018, however summer precipitation was greater in 2019. Also, the maximum lake water level was 20 cm higher in 2018. Lastly, the lake dried up later in 2019 and resurfaced following heavy precipitation on September 2.

Prior to snowmelt in late May 2019, temperatures at GS1 remained steady at ~1.3°C (Figure 7F). In 2019, after the surface water appeared in the lake, they continued rising rapidly during the following four days to 1.47 m (Figure 7E). On June 4 stream and lake temperatures reached seasonal lows of 0.9°C and 0.7°C, respectively. Daily average lake temperature proceeded to rise to 4.4°C by June 13 (Figure 7F). During this time, changes in lake water level and spring discharge corresponded to fluctuations in air temperature (Figure 7D). For example, in the first week of June daily average air temperature decreased by 10°C, lake water level decreased by 0.5 m and spring discharge decreased by 0.13 m^3 s^{-1}(Figure 7D, E, F). As air temperatures rose water levels and spring discharge recovered.

Lake water level reached a maximum of 1.62 m on June 18, 2019 and stayed high until mid-July when it began its downward trajectory (Figure 7E). The decline in lake water levels coincided with a rapid increase in both lake and stream temperatures (Figure 7F). By August 25, the lake had dried up. However, the lake briefly appeared again following precipitation on September 2, which was confirmed by a field visit on September 4. This pattern was reflected in stream temperatures as a decrease when lake water level was below the surface and an increase when it resurfaced.

4.3 Chemical and isotopic composition

As the snowpack started to melt in the catchment in late May 2019, the alkalinity at GS1 briefly fell, and spring water became depleted in deuterium (Figure 8E). This suggests the contribution of snowmelt water to the springs through infiltration, as water levels were rising (Figure 8B). However, once water levels reached a maximum in the lake on June 4, spring temperature and alkalinity began to increase, and isotopic compositions became less negative (Figure 8D). This could be due to the increased hydraulic gradients forcing pre-melt groundwater out at the springs. After July 10, alkalinity decreased with falling water levels (Figure 8).

Water samples were collected in the three spring branches and on the north shore of Hathataga Lake between August 7 and 14, 2019; and analyzed for alkalinity and major ions (Figure 9). The lake had an alkalinity of 1.8 meq L^{-1}, which was most similar to S1, the warmest spring branch, and most dissimilar to S3, the coldest spring branch.

4.4 Stream temperature

An example period (August 14–21, 2019) was chosen that included both a rain and snowfall event, and captured daily stream temperature variability, to model stream temperatures over a range of meteorological conditions (Figure 10). The first precipitation event (PE1) was a rainfall event and occurred on August 16 between 13:15 and 17:00 with a maximum 15-minute intensity of 6.7 mm h^{-1} at 14:45 and a total of 8.9 mm. The second event (PE2) was a snowfall event and occurred between 22:45 on August 16 and 03:30 on August 17 with a maximum intensity was 6.6 mm h^{-1} at 02:00 and a total of 13.8 mm (Figure 10B).

During the six-day period, stream temperatures at 0 m (T1) remained between 5.0 and 5.5 degC, whereas temperature variability became more pronounced downstream (Figure 10C). T1 was located on the eastern side of the creek at GS1 which meant that the temperature was more representative of S1 (Figure 5A). For this reason, T2 was used as the boundary condition in the HFLUX model (see below). Water temperatures reached a maximum of 6.9 degC at 246 m (T4) and 9.6 degC at 809 m (T10) at 15:00 on August 19, coinciding with a maximum air temperature for the period of 17.8 degC. A minimum air temperature of -1.4 degC was attained at 07:15 on August 17. This low did not correspond with stream temperature lows, which occurred at 02:00 on August 17, during the snowfall event. At this time water temperature was 2.9 degC at 246 m and 1.1 degC at 809 m downstream. This meant a temperature drop during the snowfall event that started at 22:45 of 2 degC and 3.5 degC, at T4 and T10 respectively (Figure 10C). During the rainfall event stream temperatures only fell by 0.5 degC at 246 m and 0.8 degC at 809 m.

Groundwater levels in P2, located at the outlet springs, rose by 7 mm during PE1 but no pronounced stream cooling was observed. During PE2 groundwater levels only rose by 1 mm (Figure 10D). The time-lapse camera captured the accumulated snow melting after sunrise.

The temperatures simulated by the HFLUX model are shown in Figure 11A for the original model and the modified model including the latent heat of fusion (Eq. 2). During the snowfall event on August 17, the modified model had a better match with observed temperature compared to the original model. This resulted in a reduction in the overall RMSE between measured and modelled stream temperatures along the study reach from 0.46 degC to 0.38 degC for August 17, and from 0.31degC to 0.29 degC for the 6-day period.

The energy fluxes computed by HFLUX is shown in Figure 11B, where positive values correspond to an energy gain by stream and negative values an energy loss. Net shortwave radiation was the major source of energy with an average of 58.9 W m^{-2}. Net longwave radiation and the sensible heat flux were mostly positive with averages of 28.7 and 1.7 W m^{-2}, respectively. For most of the period the latent heat flux was the major heat sink with an average of -11.0 W m^{-2}. This was followed by bed conduction, the smallest flux, with an average of -1.6 W m^{-2}. The direct precipitation flux was mostly negligible as there was either no precipitation or only liquid precipitation. However, the precipitation flux became the dominant energy flux during the snowfall period, reaching a minimum of -615.5 W m^{-2}, the single largest flux during the 6-day period. The average total energy flux during the period was 67.6 W m^{-2} resulting in a net increase in water temperature downstream.

Hyporheic exchange was not included in the heat transfer equation (Eq. S2-1) in HFLUX. Nevertheless, the stream temperature model had a reasonably low RMSE. Therefore, it could be inferred that either little hyporheic exchange was occurring in the system or that hyporheic exchange had a negligible effect on stream temperatures in the channel. With this in mind, a tracer test was used to quantify transient storage.

4.5 Dye tracer test

Uranine dye was released continuously at GS1 during 10:53–11:20 on June 26, 2019, and it took 4 minutes for the tracer front to travel 152 m downstream to F1, and 6.5 minutes to F2. A plateau concentration of 37-43 ppb was reached at F1 and 31-36 ppb at F2. The range in the plateau concentrations measured at each fluorometer are attributed to an inconsistent pumping rate. This is likely due to the battery not providing a consistent voltage and the decreasing head difference between the tracer solution and the stream which made pumping harder.

The breakthrough curves were analyzed using OTIS-P. A model was generated in which both F1 and F2 were considered (Figure 12). A storage zone area (A_s , Equation S1-2) of 0.11 m^2 and 0.18 m^2, and an exchange coefficient (α, Equation S1-1 and S1-2) of $2.2\times10^{-4}s^{-1}$ and 3.0×10^{-4} s^{-1} were estimated for the respective sub-reaches. A dispersion coefficient of 1.2 m^2 s^{-1} and 1.3 m^2s^{-1}, and stream cross sectional area of 0.33 m^2 and 0.36 m^2 were also estimated. The average stream cross sectional area from stream survey measurements was 0.36 m^2. This means the storage zone area was between one-third and one-quarter the stream cross sectional area. The rate of longitudinal dispersion was comparable to estimates by Haggard et al. (2001) where flow conditions were similar. This was on the higher end of values reported in the literature (0.05 – 1.3 m^2 s^{-1}) (Lautz & Siegel, 2007). The RMSE of the model was 0.93 ppb. The plateau concentrations were used to account for tracer dilution. Discharge increased by 0.042 m^3 s^{-1} or 25 % between GS1 and GS2. Discharge increases of 0.018 m^3 $s^{-1}$and 0.024 m^3 s^{-1} were determined for the respective sub-reaches. Discharge obtained from the GS1 and GS2 rating curves showed an increase of 28% along the reach (Figure 3) which is similar to the estimates obtained through tracer dilution. The average time that solutes spent in the storage zone (t_s) was 18 minutes suggesting that transient storage represents storage in the hyporheic zone, which can retain some solutes for 10-30 minutes, rather than stagnant side channel. This is complemented by field observations of turbulent flow with few stagnant pools.

Hyporheic exchange in the channel therefore did not have a noticeable effect on stream temperatures and represented a negligible flux compared to the energy fluxes included in the heat transfer equation (Equation S2-1). Furthermore, hyporheic exchange is likely captured in part by the bed conduction flux (Equation S2-11).

5. Discussion

5.1 Lake and spring thermal and hydrogeologic connectivity

The headwater springs of Hathataga Creek is thermally influenced by the seasonal body of water in the lake located upgradient of the springs, resulting in a strong seasonality in the temperature of spring discharge, which in turn affects the stream thermal regime (Figurer 13). The spring has a steady temperature of ~1.3 °C during winter and early spring while the lake is covered by snow (Figure 7). As the water table rises under the lake and forms the surface water body after snowmelt, the lake becomes an effective absorber of shortwave radiation. As a result, the lake water temperature rises, and so as the temperature of S1 spring receiving the water sourced by the lake (Figure 13A). S2 and S3 springs receive less of lake-influenced groundwater but more of the groundwater that bypasses the lake. This results in a temperature contrast between S1 and S2/S3 (Figure 5). As the lake dries out towards the end of the summer (Figure 13B), the spring temperature decreases rapidly due to the loss of warm water from the lake.

The distinct thermal characteristics of lake-headed stream temperatures have previously been described (Dripps & Granger, 2013; Garrett, 2010; Mellina et al., 2002). This study presents a unique example of an indirectly lake-headed stream i.e., where the interaction of groundwater and lake water, and the hydraulic gradient determine the resulting stream temperature.

The processes taking place in this system have important implications for the stream thermal regime under a changing climate. There have been greater than average regional increases in mean air temperatures on the eastern slopes of the Canadian Rockies. Warming of 2.6 °C has been recorded at the Marmot Creek research basin, located 15 km north of the Hathataga valley, since the 1960s (Harder, Pomeroy, & Westbrook, 2015; Fang & Pomeroy, 2020). Typically, the concern is that this leads to stream warming (Leach & Moore, 2019). Higher summer air temperatures in the Hathataga valley would lead to higher lake temperatures and therefore even greater stream warming. Earlier snowmelt (Stewart, Cayan, & Dettinger, 2005) and a reduced snowpack (Mote, Hamlet, Clark, & Lettenmaier, 2005) have also been shown for the region. Reduced summer streamflows would exacerbate stream warming. However, the duration of the surface water in the lake would be shortened due to a reduced snowpack. This in turn would reduce the time of warm groundwater contribution to the springs, resulting in stream cooling. On the other hand, summer precipitation has been increasing in the Canadian Rockies (Harder et al., 2015). Increased summer precipitation could also impact the lake's hydroperiod by increasing lake water levels and extending the life of the lake. The frequency of mid-winter melts is also likely to increase into the future (O'Neil, Prowse, Bonsal, & Dibike, 2017). This could cause a lake-spring connection in winter months. Climate change will therefore impact the timing and magnitude of lake water levels, which are an important control on stream temperatures.

This study illustrates the complex and non-linear nature of climate change on surface water-groundwater interactions and the need to further study the effects of both intermittent and non-intermittent alpine lakes on stream thermal regimes.

5.2 Effects of direct precipitation on stream temperature in cold regions

Previous studies have concluded the direct precipitation heat flux to be negligible (Evans et al., 1998) and observed stream cooling has been attributed to the resulting flow generation processes (Brown & Hannah, 2007). We began this study with the aim of quantifying these subsurface flows to improve stream temperature models. However, we found that direct precipitation made up a large component of the energy balance during solid precipitation events (Figure 11B) consistent with the findings of Leach and Moore (2017). Furthermore, Hathataga Creek did not undergo any noticeable cooling during rainfall events. This suggested that an increase in advective inputs, from groundwater and hillslope pathways, did not play an important role in altering stream temperatures.

The stream energy balance was dominated by shortwave radiation during the day and longwave radiation at night (Figure 11B). The largest temperature residuals occurred between 14:00 and 15:00 when measured temperatures were up to 1.5 °C warmer than modelled ones. The uncertainties in shortwave radiation came from estimates of shading. This is attributed to shading values that were fixed in the model and therefore did not change throughout the day. The radiation measurements were taken in an open meadow. For most of the day the stream was well shaded as captured by the shading estimates. However, in mid-afternoon the position of the sun was such that it shone along the length of the stream and shading estimates became erroneous. In future modelling studies, shading and view to sky coefficient should be quantified in the field using hemispherical images (Garner, Malcolm, Sadler, & Hannah, 2017) or a densiometer (Gravelle & Link, 2007).

Uncertainties in longwave radiation came from the assumption that canopy surface temperature equals air temperature. In reality, longwave radiation from surrounding vegetation (L_{veg}, Equation S2-5) is likely greater on sunny days when canopy temperature is greater than air temperature (Pomeroy et al., 2009). The remaining fluxes were relatively small in comparison. Uncertainties in the latent and sensible heat flux came from meteorological measurements made at 3.45 m height rather than 2 m. As a result, wind speed and the latent heat flux were likely lower. Furthermore, measurements were made over the meadow rather than the stream surface. It has been shown that wind speed is higher and more variable at exposed regional weather stations compared to sheltered microclimate sites (Benyahya, Caissie, El-Jabi, & Satish, 2010). In this study the stream surface is located in a topographic low relative to the meadow. Therefore, wind speed was likely lower than measured. During the snowfall event the direct precipitation flux was ten times greater than other energy inputs.

The energy consumption caused by the melt of solid precipitation have important implications for stream temperatures in alpine environments and other cold regions. Equation 2, which describes this process, should be considered in stream energy balance models. Without this flux, parameter estimates from calibration would be less reliable to account for the lower stream temperatures. In other mountain regions, such as the Vernagtbach basin in Austria, there are years when solid precipitation accounted for up to 70 percent of total precipitation during the ablation season. During the same period, there were up to 50 days with snowfall (Escher-Vetter & Siebers, 2007). In the Hathataga catchment, solid precipitation accounted for 23 percent of total precipitation from May to September 2019 with 20 days of snowfall.

This could also have important implications for the field of meteorology where it is a challenge to determine precipitation phase. Greater than expected temperature changes in small streams or of fluid in a precipitation gauge (Geonor, T-200B) could be used as a proxy for solid/liquid phase rather than using an air temperature threshold or expensive laser-based sensors (Campbell Scientific, CS125). The advantage of this method is that cooling associated with the latent heat of fusion only occurs for solid precipitation, irrespective of air temperature. This was especially relevant during summer hailstorms when surface air temperatures were up to 10 °C but stream cooling was observed.

6. Conclusions

Hathataga Creek is sourced by a spring complex located downgradient of a seasonal lake, Hathataga Lake. It represents an example of groundwater-fed headwater streams in mountain regions. The spring complex consists of three separate springs having different thermal regimes, which are strongly influenced by the hydroperiod of Hathataga Lake. When the lake is dry, the temperatures of the three springs are equal and controlled by groundwater temperature in the catchment. However, once the lake forms, following snowmelt, the temperature of the spring receiving lake-influenced groundwater rises compared to other springs. During the summer months, lake water level and the lake energy balance determine the magnitude and temperature of the water flux from the lake to the springs. Climate change will likely result in changes to the conditions that control the hydroperiod of the lake, namely the depth of snowpack, the timing of snowmelt, amounts of summer precipitation, and lake-atmosphere energy exchange. Therefore, groundwater-lake water interactions must be considered when predicting future stream temperatures in these settings.

The energy balance of the stream reach below the headwater springs was mainly controlled by shortwave and longwave radiation. However, stream temperature decreased rapidly during snowfall events due to direct entry of snowfall onto the stream surface and subsequent melting. Stream temperature models are improved when the latent heat flux associated with the melting of direct snowfall are included. This process is especially relevant in winter months and in cold regions where summer snowfall and hailstorms are common. Tracer tests indicated substantial effects of hyporheic exchange, but its effects on stream temperature was negligible implying that energy exchange by hyporheic processes played insignificant role in this particular setting.

Further case studies should be conducted on both seasonal and perennial lakes to assess the effect of groundwater-lake water interactions on stream temperatures downgradient. For the assessment of climate-change impacts on headwater stream temperatures, it will be beneficial to use physically-based catchment models including snow accumulation and melt, energy balances of streams and lakes, and subsurface energy transfer between streams and lake.

Acknowledgement

We thank Jesse He, Brandon Hill, Evan Sieben, and numerous others of assistance with field work; Edwin Cey and Jason Leach for constructive comments on an earlier draft, John Pomeroy and the University of Saskatchewan's Cold Water Laboratory for sharing hydro-meteorological data, and the Fortress Mountain Resort and the University of Calgary's Biogeoscience Institute for logistical supports. Funding for this study was provided by Canada First Research Excellence Fund (Global Water Futures), Alberta Innovates (Water Innovation Program), Natural Sciences and Engineering Research Council, and the Graduate Students Association of the University of Calgary.

Hosted file

`References.pdf` available at https://authorea.com/users/411972/articles/520821-hydrogeological-control-of-the-thermal-regime-of-a-sub-alpine-headwater-stream

Hosted file

`Electronic supplementary material.pdf` available at https://authorea.com/users/411972/articles/520821-hydrogeological-control-of-the-thermal-regime-of-a-sub-alpine-headwater-stream

Hosted file

`Tables.pdf` available at https://authorea.com/users/411972/articles/520821-hydrogeological-control-of-the-thermal-regime-of-a-sub-alpine-headwater-stream

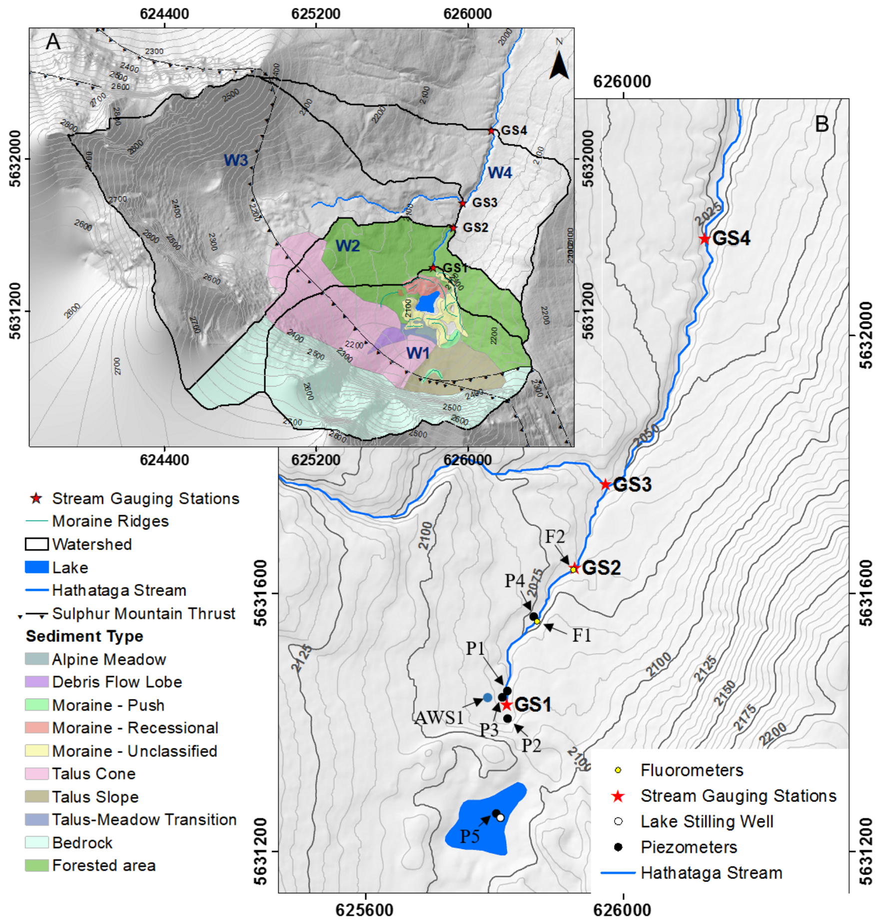
A
W1
W2
W3
W4
GS1
GS2
GS3
GS4
Stream Gauging Stations
Moraine Ridges
Watershed
Lake
Hathataga Stream
Sulphur Mountain Thrust
Sediment Type
Alpine Meadow
Debris Flow Lobe
Moraine - Push
Moraine - Recessional
Moraine - Unclassified
Talus Cone
Talus Slope
Talus-Meadow Transition
Bedrock
Forested area
B
F1
F2
P1
P2
P3
P4
P5
AWS1
Fluorometers
Stream Gauging Stations
Lake Stilling Well
Piezometers
Hathataga Stream
624400
625200
626000
625600
5632000
5631600
5631200

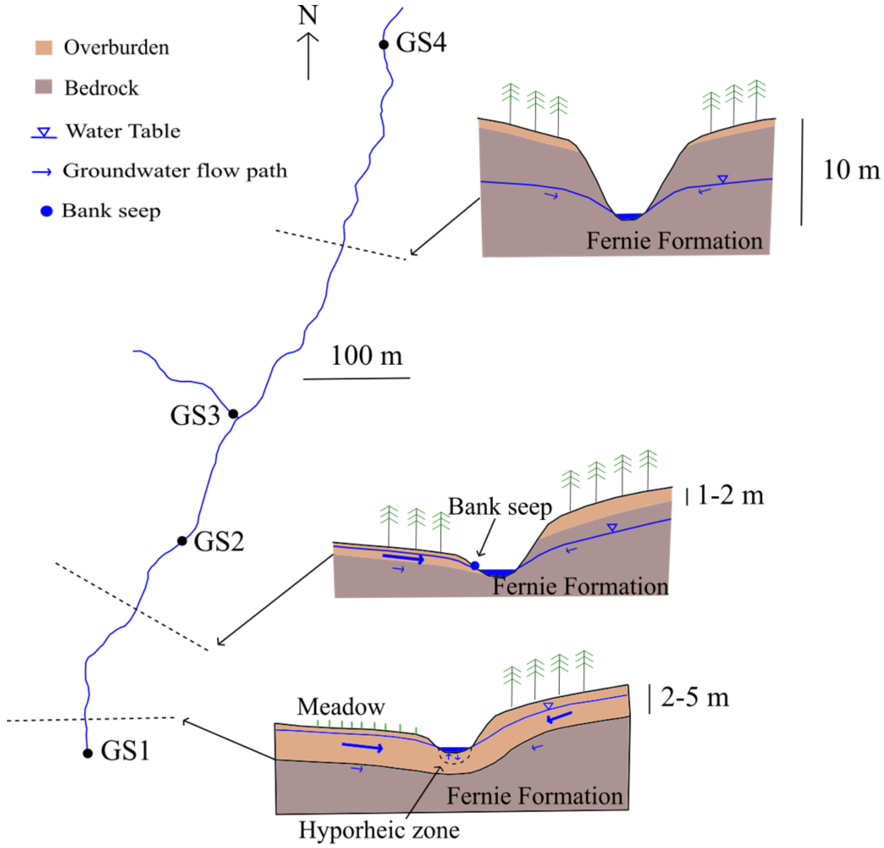

N
Overburden
Bedrock
Water Table
Groundwater flow path
Bank seep
GS4
10 m
Fernie Formation
100 m
GS3
Bank seep
1-2 m
GS2
Fernie Formation
Meadow
2-5 m
GS1
Fernie Formation
Hyporheic zone

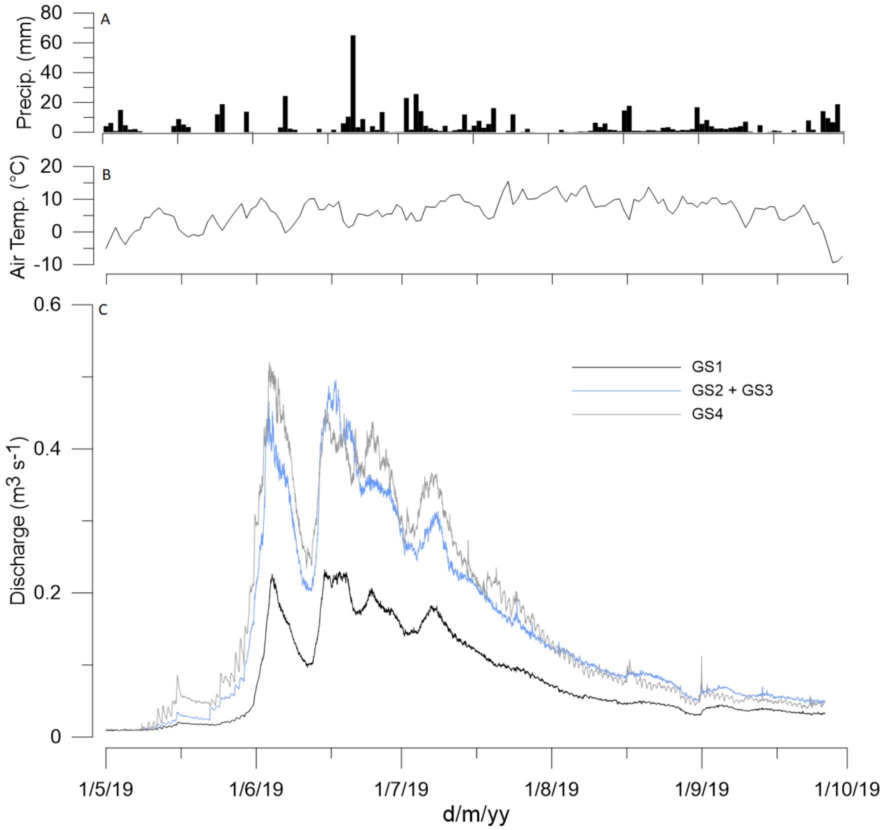
A
Precip. (mm)
0
20
40
60
80
B
Air Temp. (°C)
-10
0
10
20
C
Discharge (m3 s-1)
0
0.2
0.4
0.6
GS1
GS2 + GS3
GS4
1/5/19
1/6/19
1/7/19
1/8/19
1/9/19
1/10/19
d/m/yy

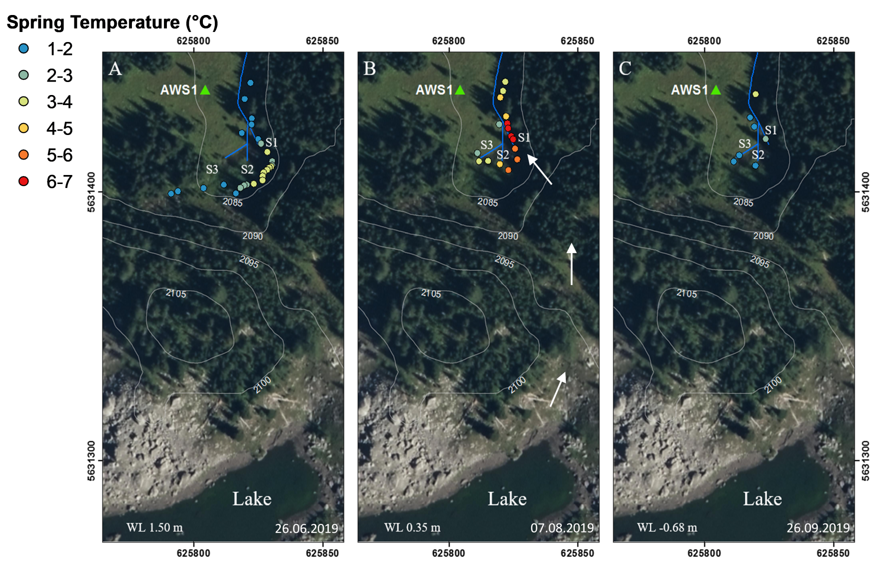
Spring Temperature (°C)
1-2
2-3
3-4
4-5
5-6
6-7
A
B
C
AWS1
S1
S2
S3
2085
2090
2095
2100
2105
Lake
WL 1.50 m
26.06.2019
WL 0.35 m
07.08.2019
WL -0.68 m
26.09.2019
625800
625850
5631400
5631300

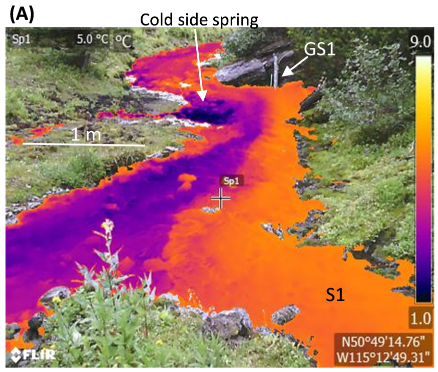
(A)
Cold side spring
GS1
Sp1
5.0 °C
1 m
S1
9.0
1.0
N50°49'14.76"
W115°12'49.31"

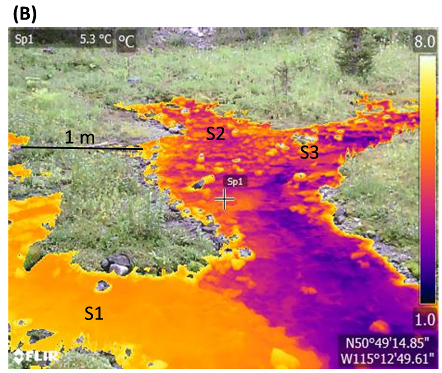
(B)
Sp1
5.3 °C
1 m
S2
S3
S1
8.0
1.0
N50°49'14.85"
W115°12'49.61"

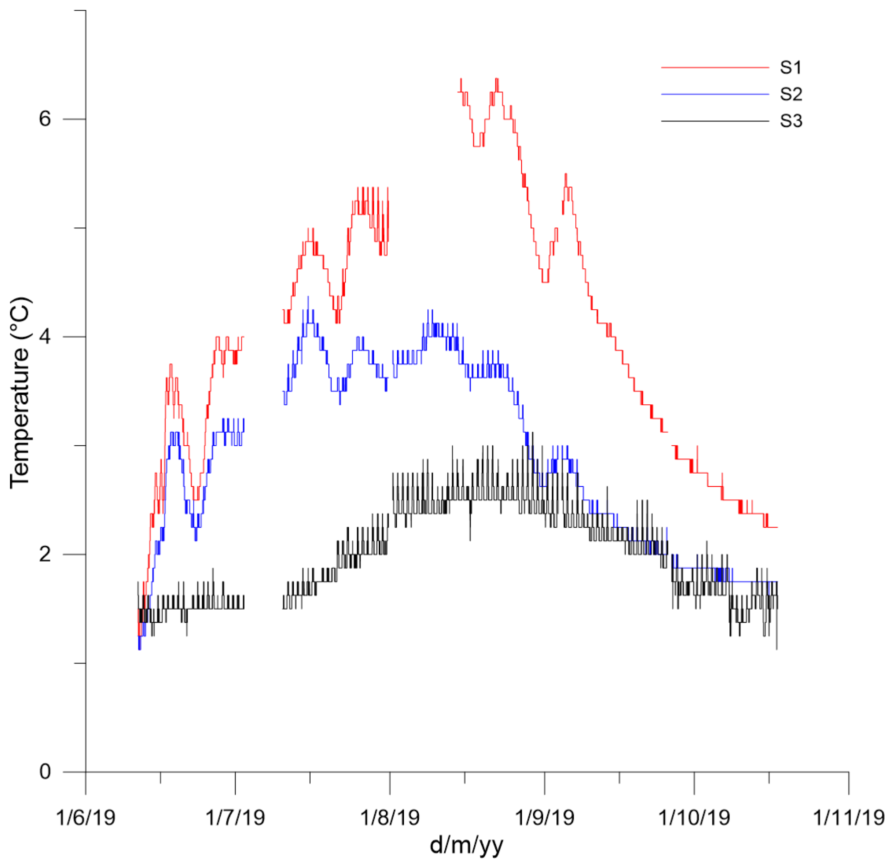
S1
S2
S3
Temperature (°C)
0
2
4
6
1/6/19
1/7/19
1/8/19
1/9/19
1/10/19
1/11/19
d/m/yy

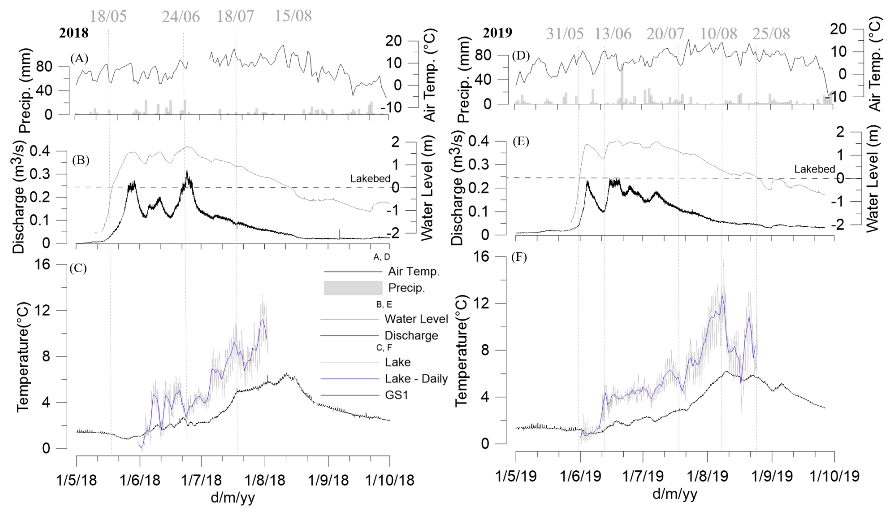
2018
18/05
24/06
18/07
15/08
(A)
Precip. (mm)
Air Temp. (°C)
(B)
Discharge (m3/s)
Water Level (m)
Lakebed
(C)
Temperature(°C)
A, D
Air Temp.
Precip.
B, E
Water Level
Discharge
C, F
Lake
Lake - Daily
GS1
1/5/18
1/6/18
1/7/18
1/8/18
1/9/18
1/10/18
d/m/yy
2019
31/05
13/06
20/07
10/08
25/08
(D)
(E)
(F)
1/5/19
1/6/19
1/7/19
1/8/19
1/9/19
1/10/19

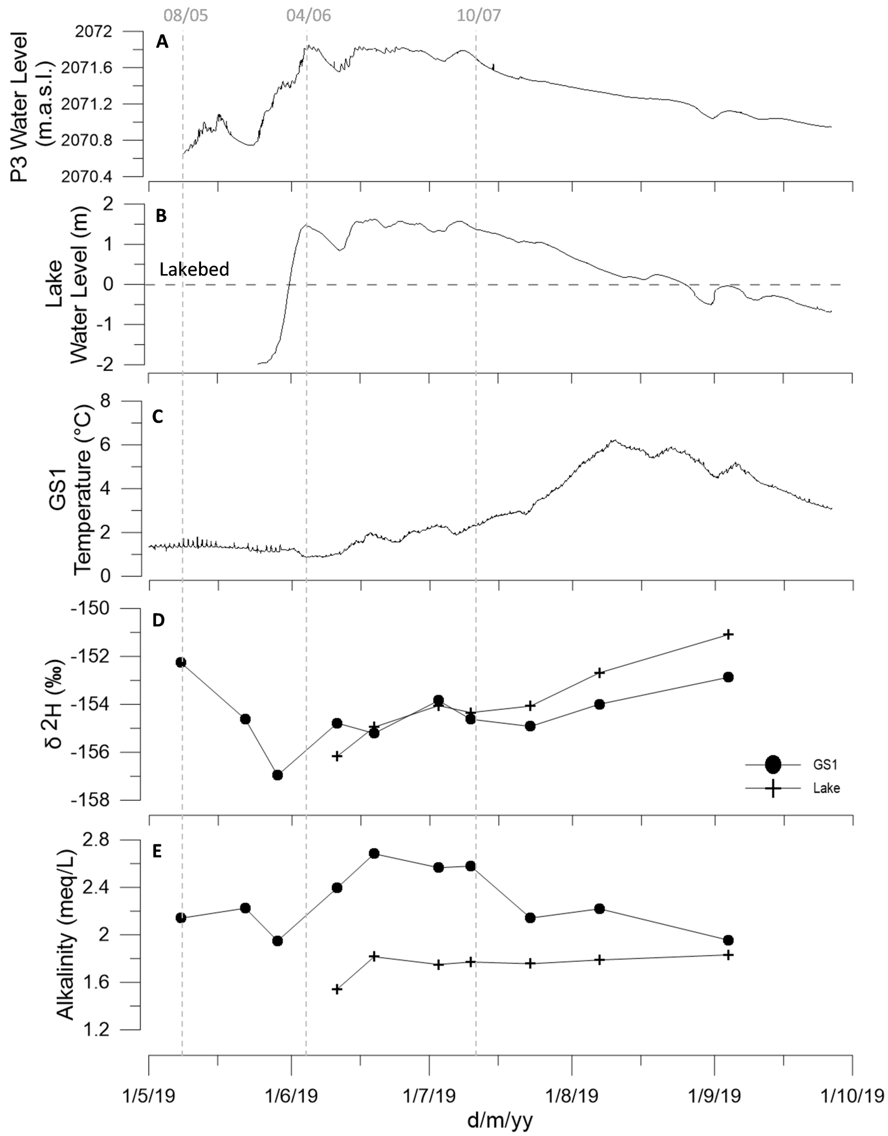
08/05
04/06
10/07
A
P3 Water Level (m.a.s.l.)
B
Lake Water Level (m)
Lakebed
C
GS1 Temperature (°C)
D
δ 2H (‰)
GS1
Lake
E
Alkalinity (meq/L)
1/5/19
1/6/19
1/7/19
1/8/19
1/9/19
1/10/19
d/m/yy

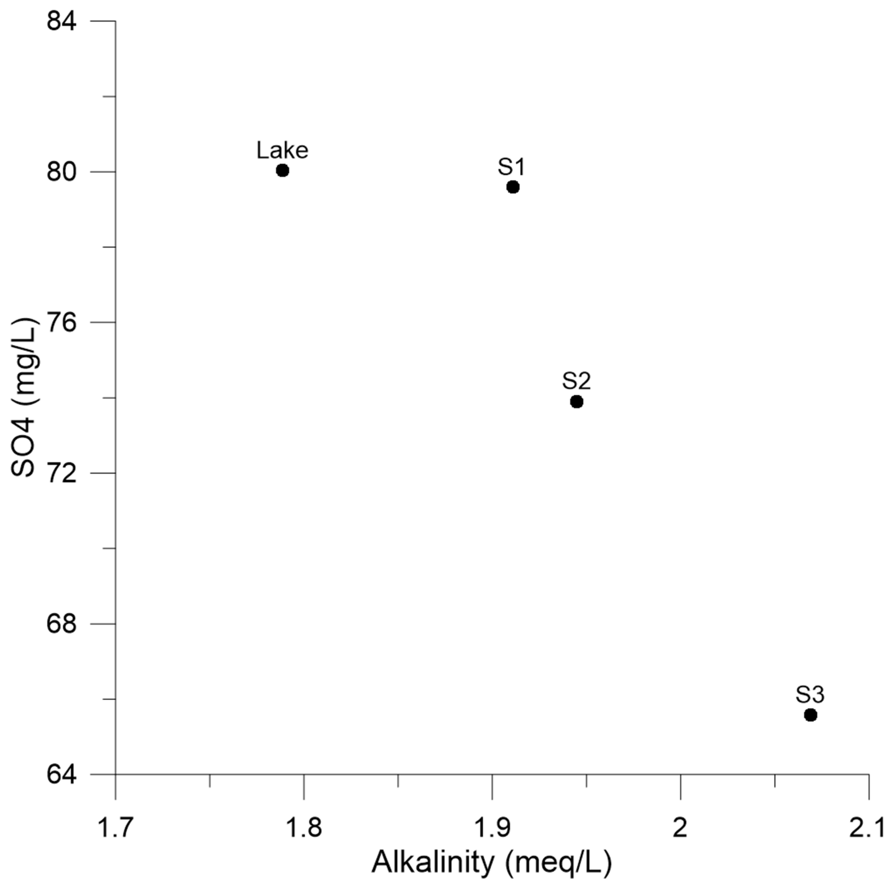
84
80
76
72
68
64
SO4 (mg/L)
Lake
S1
S2
S3
1.7
1.8
1.9
2
2.1
Alkalinity (meq/L)

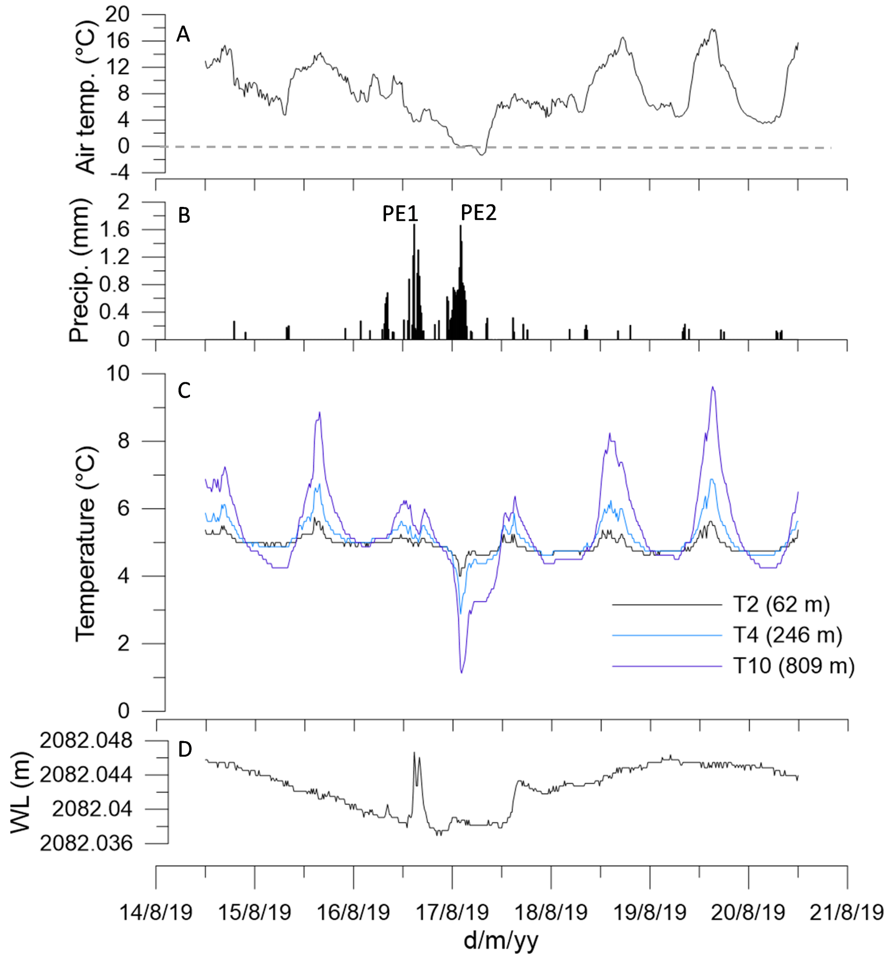

A
Air temp. (°C)
20
16
12
8
4
0
-4
B
PE1
PE2
Precip. (mm)
2
1.6
1.2
0.8
0.4
0
C
Temperature (°C)
10
8
6
4
2
0
T2 (62 m)
T4 (246 m)
T10 (809 m)
D
WL (m)
2082.048
2082.044
2082.04
2082.036
14/8/19
15/8/19
16/8/19
17/8/19
18/8/19
19/8/19
20/8/19
21/8/19
d/m/yy

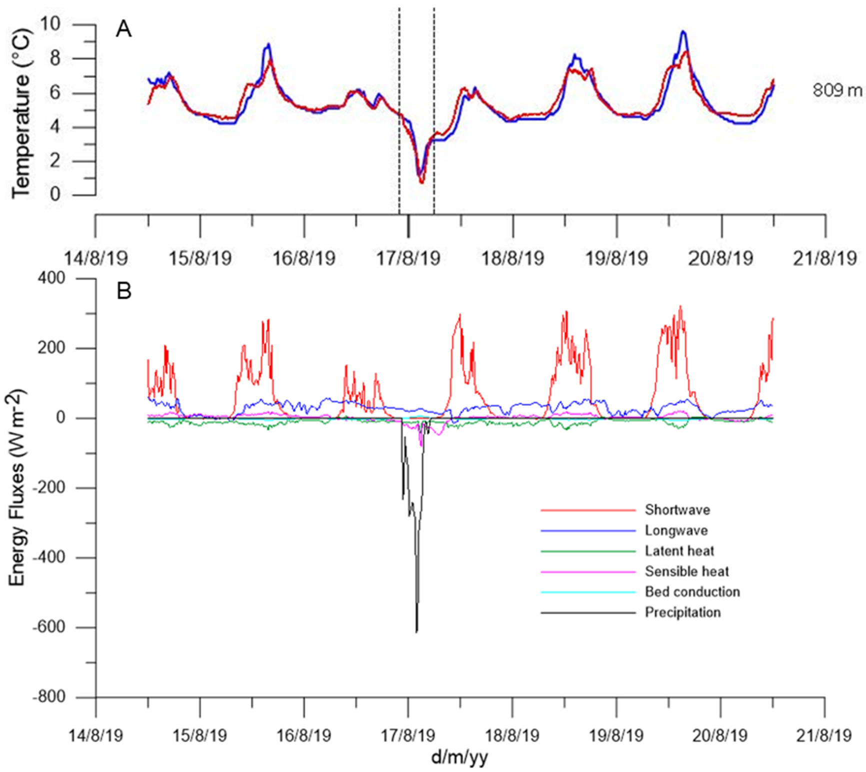
A
Temperature (°C)
809 m
14/8/19
15/8/19
16/8/19
17/8/19
18/8/19
19/8/19
20/8/19
21/8/19
B
Energy Fluxes (W m-2)
Shortwave
Longwave
Latent heat
Sensible heat
Bed conduction
Precipitation
d/m/yy

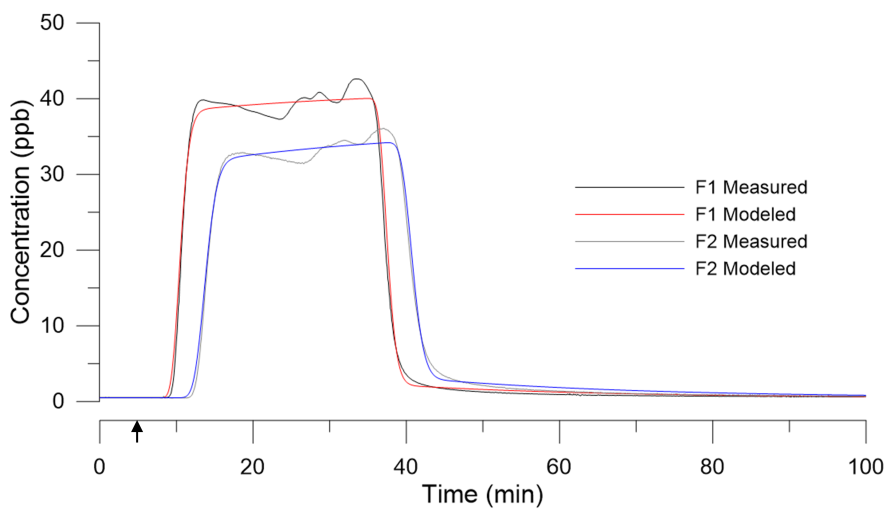
Concentration (ppb)
F1 Measured
F1 Modeled
F2 Measured
F2 Modeled
Time (min)

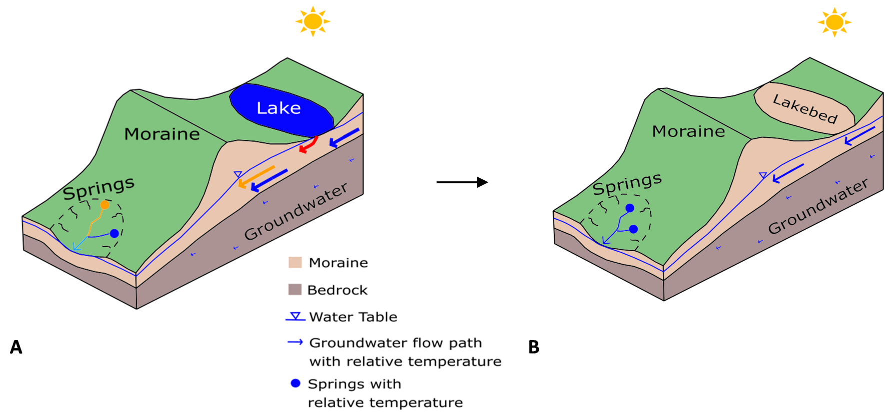
Lake
Moraine
Springs
Groundwater
Lakebed
Moraine
Springs
Groundwater
Moraine
Bedrock
Water Table
Groundwater flow path
with relative temperature
Springs with
relative temperature
A
B